Supporting Information

Pseudo-bilayered inverted organic solar cells using Marangoni effect

Jihwan Jo, Seonju Jeong, Dongchan Lee, Seungjin Lee, Bumjoon J. Kim, Shinuk Cho, and Jung-Yong Lee*

Experimental method

Materials. All devices were deposited on the prepatterned ITO/glass with a sheet resistance of 16 Ω sq^{-1} from AMG. The PM6 polymer and Y7-BO small-molecule were purchased from Derthon and 1-materials, respectively. All other materials, such as ZnO precursors, chlorobenzene (CB), and chloronaphthalene (CN), were purchased from Sigma Aldrich.

OSC devices fabrication. The devices were fabricated with an inverted structure of ITO / ZnO / active layer / MoO_x / Ag. The ITO/glass substrates were pre-cleaned by detergent, acetone, and IPA in a sonicator and were UV-treated in an ozone chamber. For the ETLs, the ZnO solution (zinc acetate 1g, ethanol amine 0.0280g, and 2-methoxy ethanol 1ml) was dropped for SC at 6000 rpm, and then the substrates were heated to 200℃ for 30 minutes in the air. For the BHJ active layers, the PM6:Y7-BO solution (20mg in CB with 0.5% CN; D/A ratio was 1:1.5) was dropped for SC at 1500 rpm. The Y7-BO solution (10mg in CF) was dropped for SC at 3000 rpm for the PB active layer. The PM6 solution (15mg in CB with 3.8% CN) was dropped by 16 μl onto the water for SS, and the spread PM6 films were transferred onto the Y7-BO films after the CB was almost evaporated. The samples were heated on a hotplate at 120℃ for 1 minute immediately after the transfer. The heating time was kept very short to minimize the effect of heating on the morphology of the films without the excessive phase separation by the solvent additive. For the HTL and top electrode, the MoO_x and Ag were thermally evaporated in a vacuum. Lastly, for the further optimization, the ZnO layer was passivated by spin-coating a 1,2-ethanedithiol (EDT; 0.1 v/v% in acetonitrile) solution onto the ZnO layer at 6000 rpm for 30 s. No additional thermal treatment was performed after the spin-coating process.

Measurement for the morphological and electrical properties. The topology and cross-session images were obtained using AFM (MultiMode 8, Bruker) in a ScanAsyst mode under

ambient conditions and TEM (FEI Titan cubed G2 60–300, 80 keV (Titan Double Cs corrected)). The depth profiles were extracted from TOF-SIMS measurement (TOF-SIMS5, ION-TOF GmbH). For nanomorphology, GIWAXS scan was performed using X-rays with a wavelength of λ = 1.13 Å at the PLS-II 9A U-SAXS beamline of the Pohang Accelerator Laboratory (PAL) in Korea. The *J–V* characteristics of the devices were measured using a Keithley 2400 source meter under 1 sun illumination with an AM 1.5G solar spectrum (Sciencetech) from a Xe lamp (Solar Light Company), which is calibrated by a reference Si cell (Newport). The aperture size was 0.0625 cm2. The EQE and absorption were measured using a spectral measurement system K3100 IQX (McScience) Transient photo current and voltage properties were measured using a 540 nm light source, and additionally, a white LED was used as a background for the TPV measurement. The FTPS-EQE was measured in an in-house built FTPS-EQE setup, consisting of an INVENIO-R spectrometer (Bruker) equipped with a quartz beam splitter, and tungsten-halogen lamp. EL spectra were collected by MAYA2000 PRO spectrophotometer (Ocean optics)

Bilayer structure using small-molecules as bottom layers

For fabrication of a bilayer structure, a volatile solvent such as chloroform (CF) has been recently used in the subsequent spin coating (SC). Polymers are normally used as bottom layers because of their rigidity on solvents. When the CF was dropped on the PM6 film while spinning, the PM6 film was not dissolved although the CF is a good solvent for the PM6 (Figure S1). The CF was removed before entirely dissolving the PM6 film

On the other hand, the Y7 film was dissolved entirely by dropping the CF, even though the CF is a poor solvent for the Y7 (Figure S1). This vulnerability to the solvent of small-molecule films makes it very challenging to use the small-molecules as bottom layers in fabrication of the bilayer structure.

However, for the fabrication of an inverted structure that allows good stability (Figure S2), the small-molecule needs to be coated as a bottom layer. The spontaneous spreading (SS) process can allow a bilayer structure with the bottom small-molecule layer, even using the same solvent with the top layer. Figure S3 and S4 show the bilayer structure from the SS process, using chlorobenzen (CB) in the top and bottom layer. As motioned in the main text, removal of the main solvent of solution during the SS process prevented the small-molecule films from dissolving.

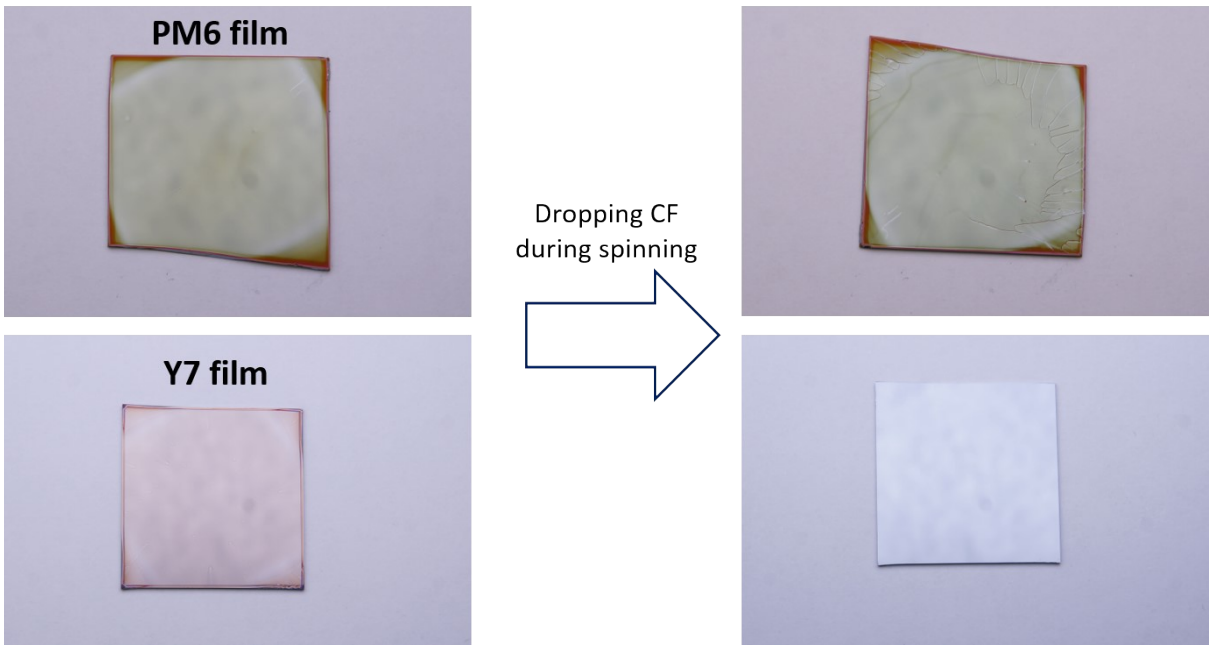

Figure S1. Dissolution of PM6 and Y7 film by dropping the CF solvent during spin.

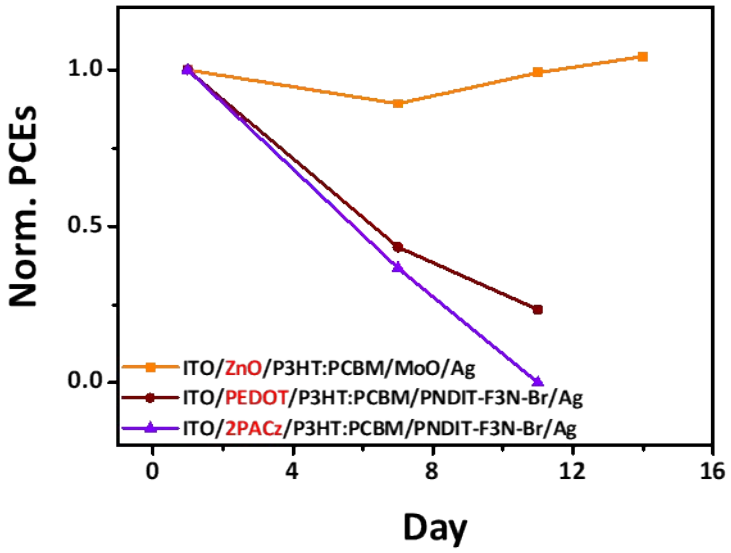

Figure S2. Stability comparison of ZnO-based, PEDOT-based, and 2PACz-based OSCs

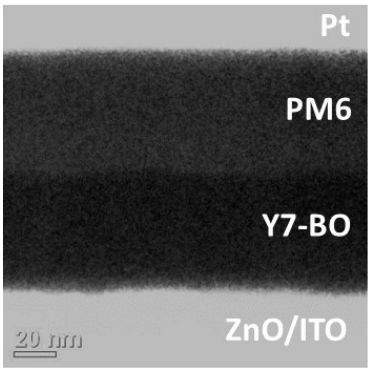

Figure S3. Cross-session image from STEM of a bilayer from the SS prcoess, by transferring PM6 film onto Y7-BO film without solvent additive.

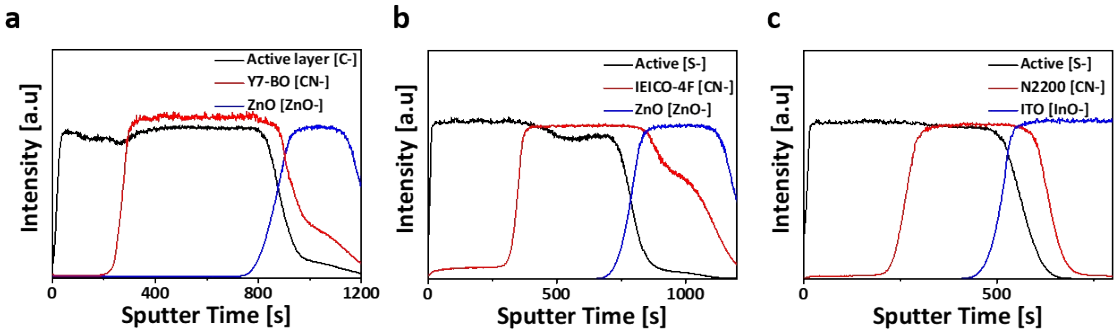

Figure S4. Depth profile from TOF-SIMS measurement of bilayered films by the SS process, by transferring **a)** PM6 film onto Y7-BO film, **b)** PTB7-Th film onto IEICO-4F film, and **c)** PTB7-Th film onto N2200 film.

Morphology of the PM6 films with and without solvent additive

Morphology parameters were extracted from images of atomic force measurement (AFM) and plots of grazing-incidence wide-angle x-ray scattering (GIWAXS) measurements. For parameters of nanomorphology from the GIWAXS scan, d-spacing and coherence length (CL) were calculated by Bragg's law ($n\lambda = 2d\sin\theta$) and Scherer equation ($CL = 2\pi K/FWHM$; K is a shape factor and close to 1), respectively. The ratio of face-on to edge-on orientation was calculated by integrating the pole figures.

To verify that the solvent additive remained within the films in the SS process, we added the solvent additive in the polymer solution and dropped 16 μl on the water, and tracked the change in interference color and weight during the evaporation of the solvent additive on the water. Figure S9a shows the stage setting for color observation. As shown in Figure S9b, spread films were floated on the water under a white LED. The white LED formed a semicircle on the films, where light from the white LED was only reflected on the upper circle. Upon spreading the solution on the water, the solvent within the films evaporated rapidly, as

shown in Figure S8. After the rapid solvent evaporation, the interference color kept changing over time and eventually stopped, forming wrinkles on the films. In addition, the videos of the interference color changes of the PM6 with the addition of 0%/1%/4%/5% CN are supplied as supplemental video 1/2/3/4, respectively.

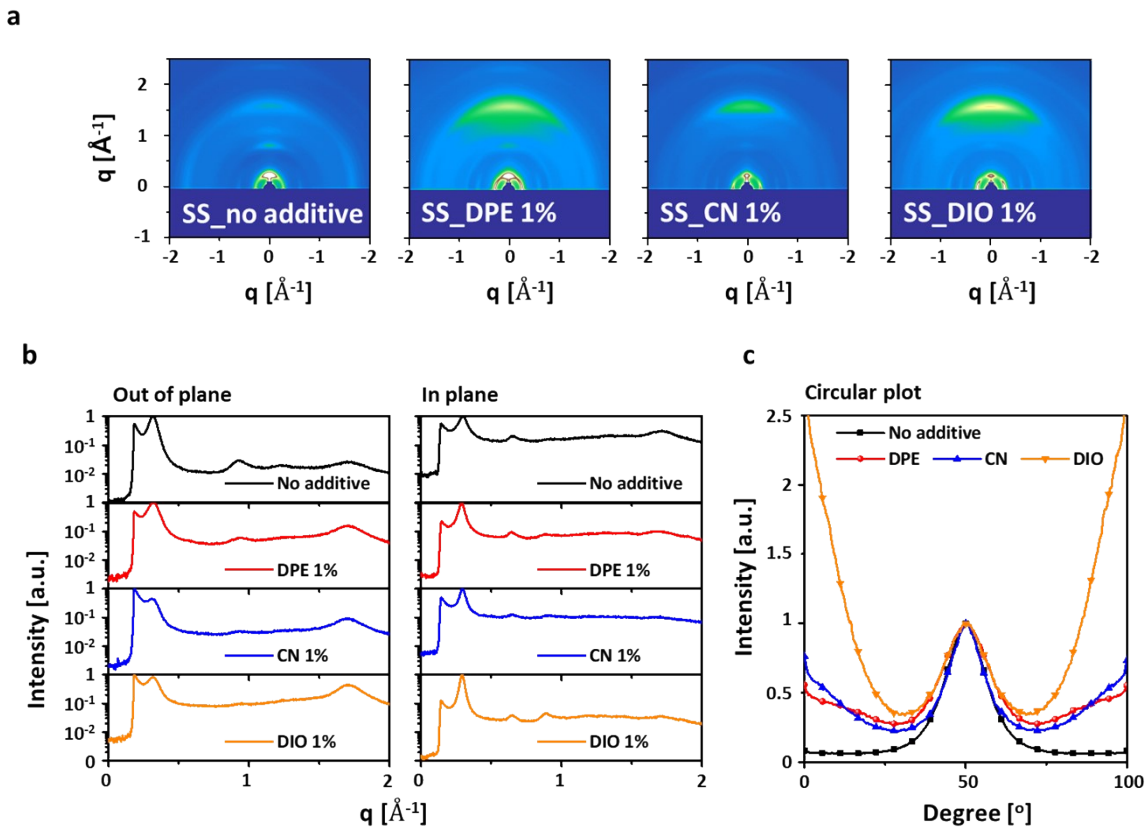

Figure S5. Nanomorphology analysis from the GIWAXS scan of the SS-PM6 films with DPE, CN and DIO. **a)** 2D images, **b)** 1D plots, and **c)** pole figures

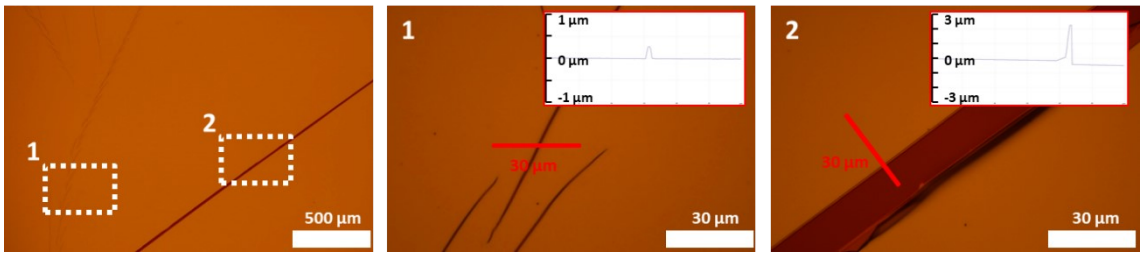

Figure S6. Optical microscope images and AFM data of the wrinkles on PM6 transferred without the CN.

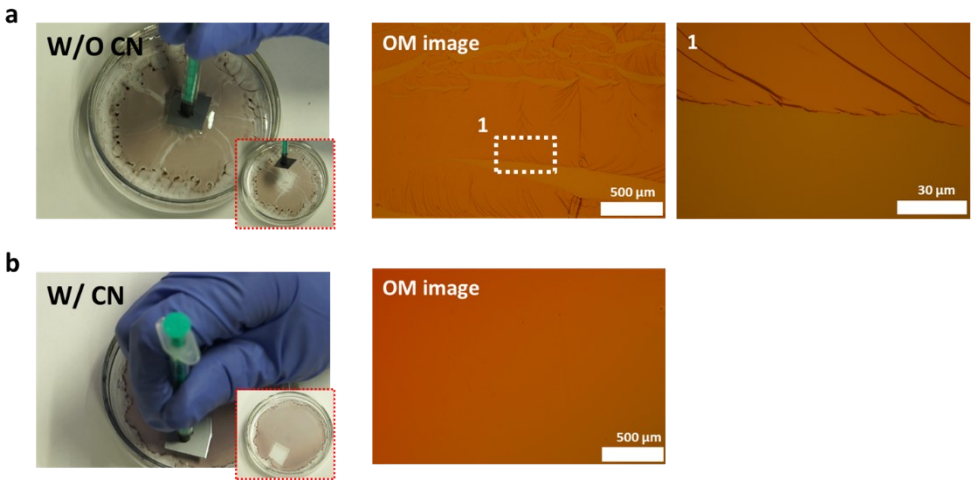

Figure S7. Photographs transferring the PFA1 and images from optical microscope (OM) of the PM6 trasnferred **a)** with the CN, and **b)** without the CN.

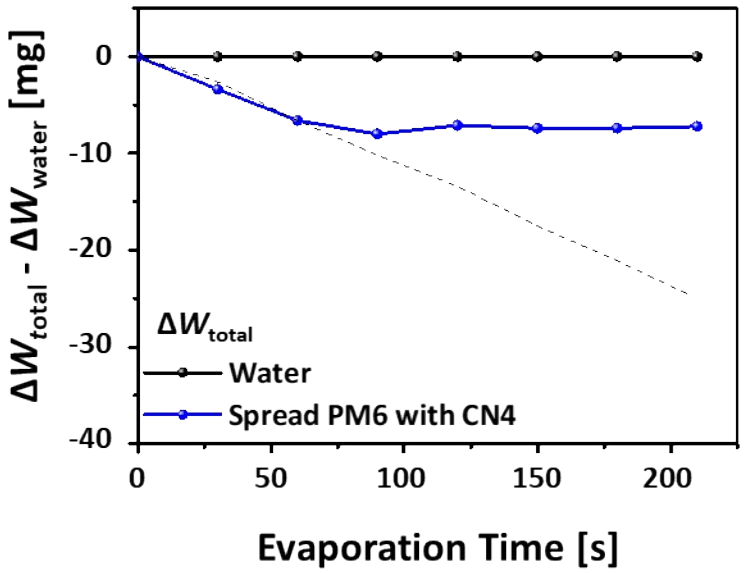

Figure S8. Weight change (ΔW) of water and PM6 film with the CN on water over time, only by the solvent evaporation; $\Delta W_{total} - \Delta W_{water}$.

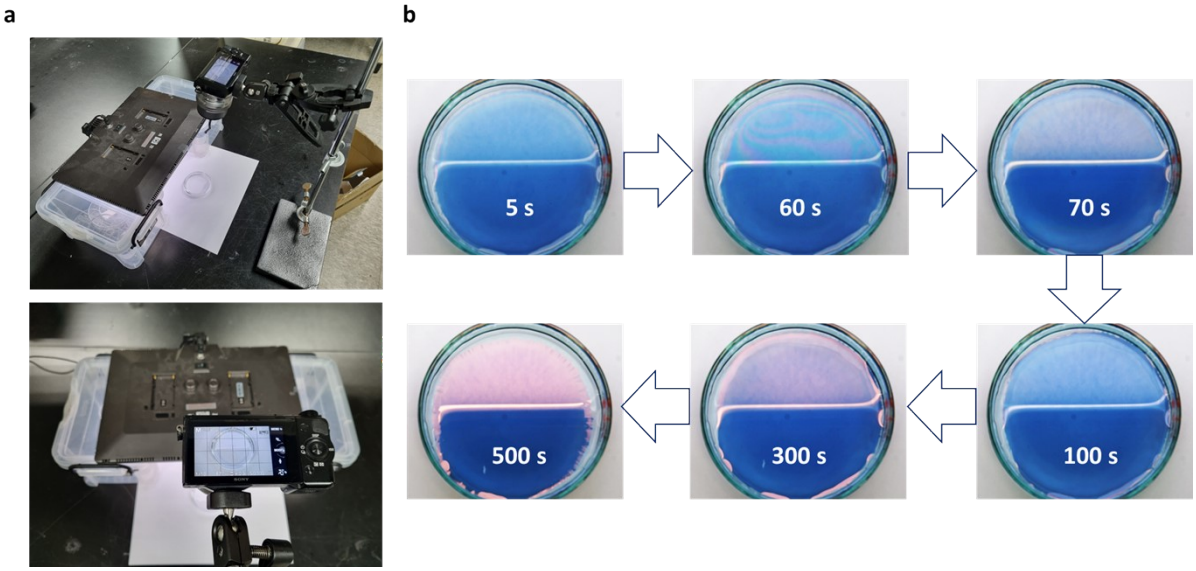

Figure S9. a) Stage set for watching the interference colors of SS-films. **b)** Spread film with the solvent additive during the SS process under the white LED over time.

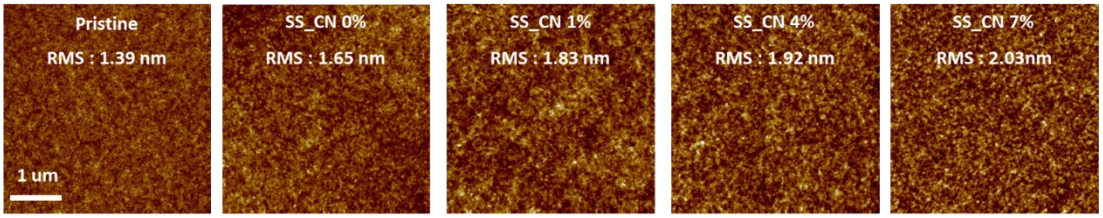

Figure S10. Topology from AFM of the PM6 film with and without the CN.

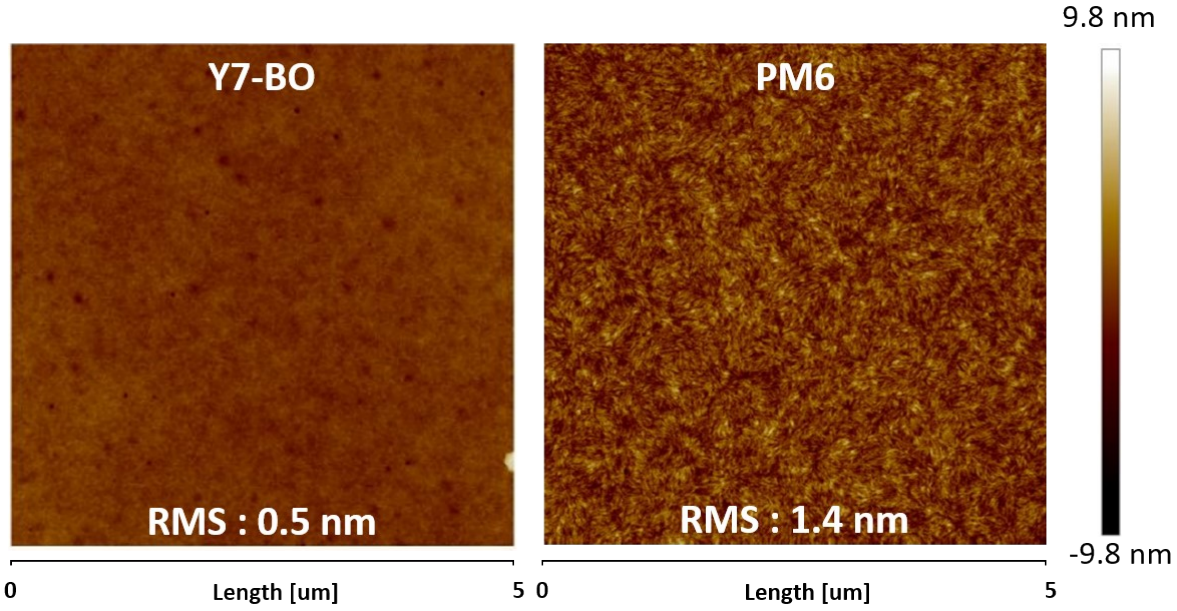

Figure S11. Topology from AFM of the pristine Y7-BO and PM6 films

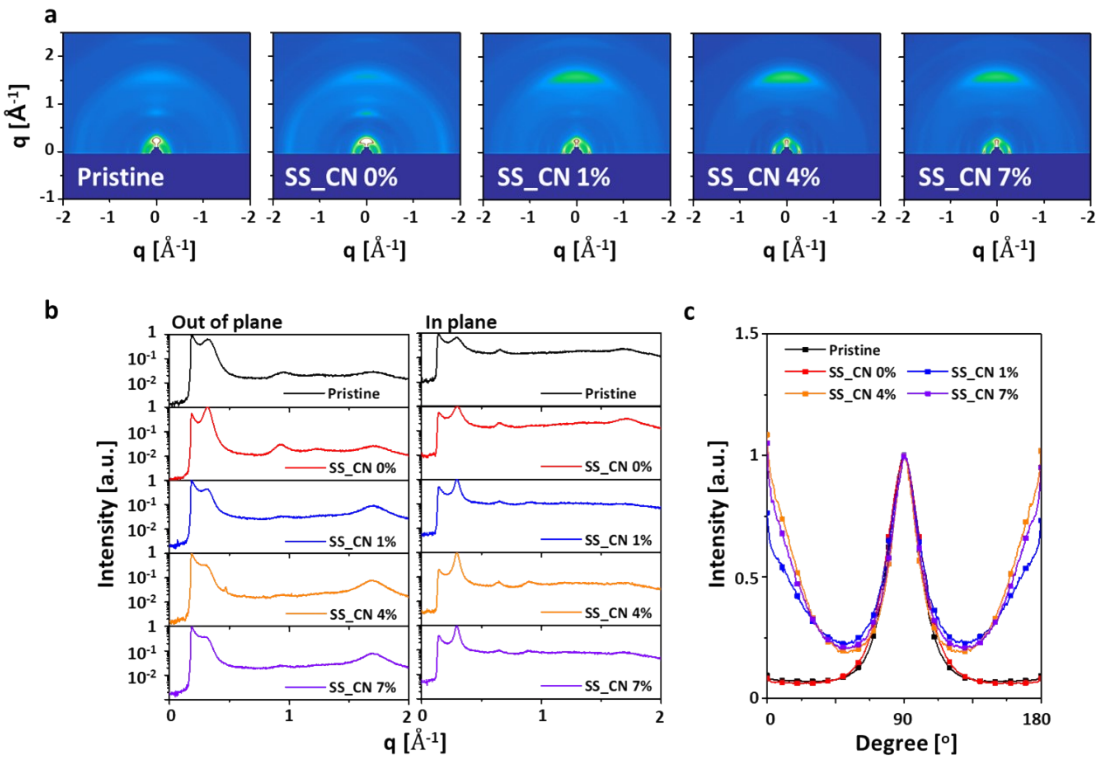

Figure S12. Morphlogy from GIWAXS scan of the PM6 films. a) 2D images, b) 1D plots, and c) pole figures.

Steady-state space-charge limited current (SCLC) method

Carrier mobility can be obtained by an SCLC method, which is described by the equation, $J = (9/8)\,\varepsilon_0\varepsilon_r\,\mu_0 V^2/d^3$, where d is the thickness of films, V is an internal voltage across the devices, μ_0 is carrier mobility, ε_0 and ε_r represent the permittivity of free space and relative permittivity, respectively. From the hole-only devices with a structure of ITO/MoO/PM6/MoO/Ag using the SCLC, the hole mobilities of the pristine PM6 and SS-PM6 films were measured (Figure S13 and Table S2). The mobility from the PM6 films with CN 4% was the fastest probably because of the crystallinity and molecular orientation. It should be noted that the PM6 with CN 7% could not be transferred onto a bottom HTL, MoO_x because of dewetting.

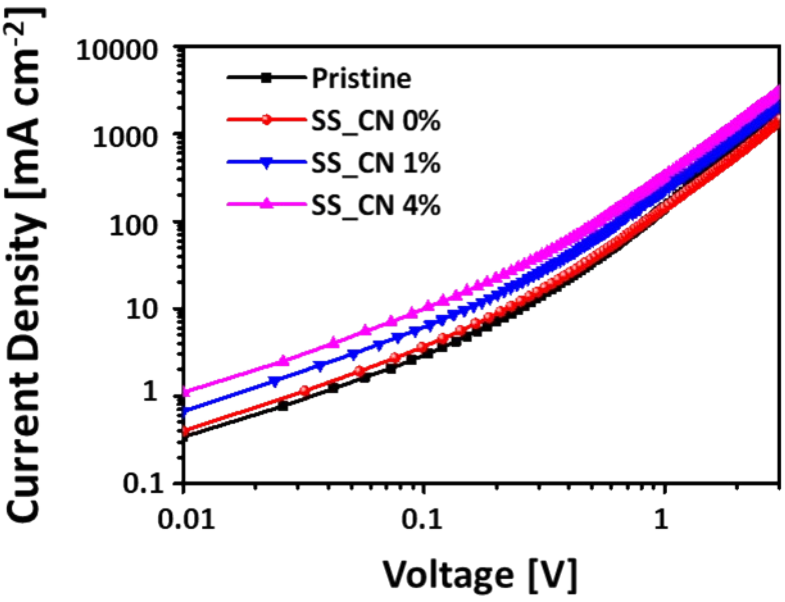

Figure S13. Dark *J-V* curves of hole-only devices (ITO/MoO_x/PM7/MoO_x/Ag) for calculating hole mobility using the SCLC method

GIWAXS scanning of the SC-PM6 with CN

The lamellar peak of the SC-PM6 films was at $q \approx 0.32$ Å^{-1} in the out-of-plane direction, consistent with the SS-PM6 films. The π–π stacking peaks in the out-of-plane direction also had a similar tendency with the addition of the CN to the SS-PM6 films. The detailed parameters of nanomorphology were summarized in Table S3

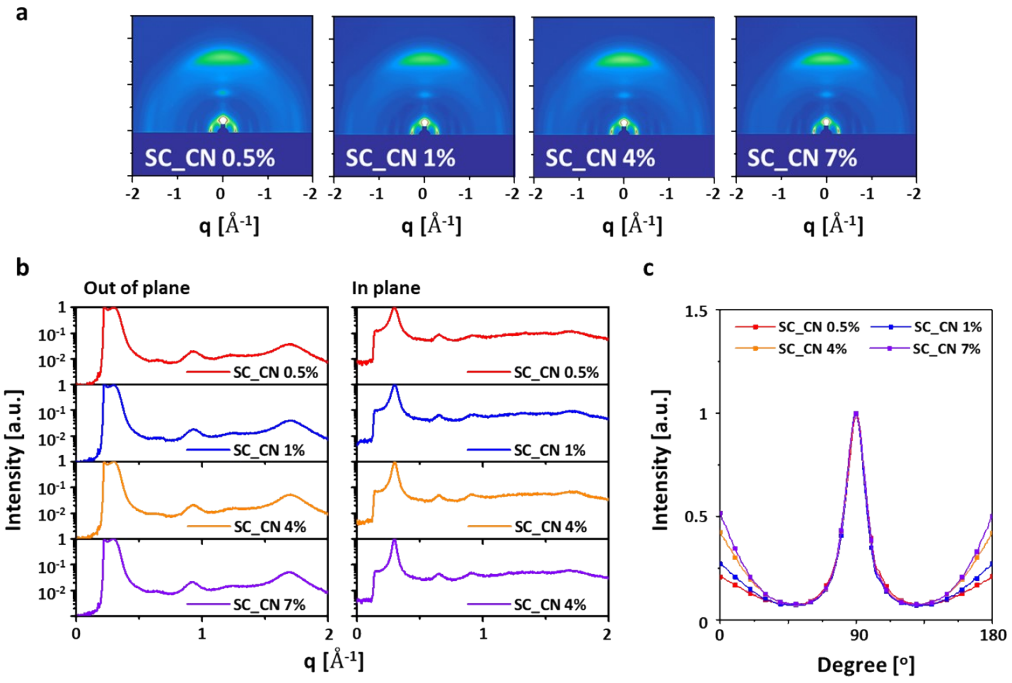

FigureS14. Morphlogy from GIWAXS scan of the SC-PM6 films with the CN. **a)** 2D images, **b)** 1D plots, and **c)** pole figures.

Optimizing the BHJ and PB OSCs

We optimized the BHJ (PM6:Y7-BO w/ CN 0.5% and total 20mg in 1ml CB) and PB (PM6 15mg w/ CN in 1ml CB, Y7-BO w/o CN and 7mg in 1ml CF) devices. In the PB devices, the thickness of the top layers (PM6 films) was controlled by the amount of dropping the PM6 solution on the water. The thickness of the bottom layers (Y7-BO films) was controlled by adjusting the concentration of the Y7-BO (Tables S4 and S5).

Fabrication of SS-PB and SS-bilayer devices by adjusting the amount of CN

We adjusted the amount of CN (0 / 1 / 4 / 7%) for the fabrication of the SS-PB devices. With the addition of the CN, the PCEs and J_{SC} rose sharply by intermixing at the D/A interfaces (Figure S15a). The performance in the samples without the CN was worst and resulted from the bilayer structure, leading to inferior exciton dissociation. The samples with CN 1% and 7% also were lower than that with CN 4% probably because of aggregation, as shown in Figure 3d.

As shown in Figure S15b, we also fabricated the bilayer structure by adjusting the dry of CN before the transfer, instead of adjusting the amount of CN. We dropped the PM6 solution with CN 3.8%, which was an optimized condition for the PB devices (Table S5). The CN was dried on the water, leaving only a very little amount of CN where the aggregation and intermix did not occur. Consequently, the overall performance of the bilayer devices by drying the CN was improved probably because of the reinforced face-on orientation and crystallinity, hence suppressing the recombination and enhancing the dissociation at the D/A interfaces. Detailed parameters were summarized in Table S6.

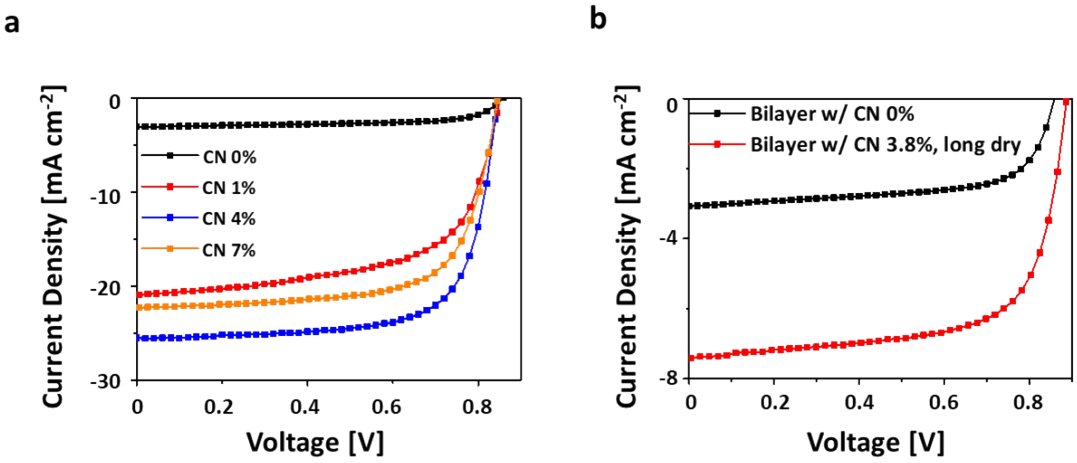

Figure S15. *J-V* characteristics of **a)** SS-PB devices by adjusting the amount of CN in the PM6 solution, and. **b)** SS-bilayer devices by adjusting the amount of CN in the PM6 solution and evaporation times of CN on the water.

Optimization in spreading of the PM6 solution using the DMSO.

For a uniform organic film, we optimized the spreading of the PM6 by adding a small amount of DMSO. The DMSO is soluble in water and has almost zero interfacial tension with water, leading to a high spreading coefficient when the droplet reaches the water. The addition of DMSO can help to spread the intrinsically non-spreading solution, as demonstrated in Figure S16. Figure S17 shows the effect of DMSO in PM6 solution with 4% CN; without the DMSO, the uniformity of PM6 film formed on the water was poor. On the contrary, the thickness became relatively uniform (45.84±2.03 nm from AFM), by adding the 0.5% DMSO into the PM6 solution. It should be noted that the amount of the DMSO was kept within 1% for the devices because of the insolubility of the PM6 solution in the DMSO, and the excessive rapid spreading. Eventually, the SS phenomenon caused by the surface tension gradient (the Marangoni effect[1-2]) was largely affected by the solvent and additive, and played the most dominant role in determining the formation of PM6 films during the SS process.

In addition, during the process of solvent evaporation and solidification, the SS process can also undergo a common mechanism, a mass transfer phenomenon as in other solution-processes (e.g., spray and inkjet coating). The mass transfer, caused by the Marangoni and capillary effects, should be carefully controlled in industrial large-area processes.[3]

It is important to also take into consideration other mechanisms, such as solvent exchange[4] and film bursting[5], under certain conditions. Additionally, the mechanical issue (e.g., winkles and cracks) in organic films can occur in the absence of the residual solvent.

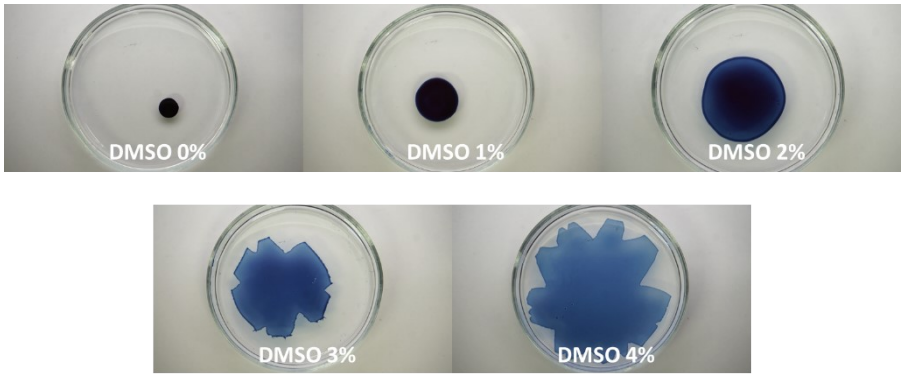

Figure S16. Spreading of the PM6 solution with CB/CN (1:1) along with the amount of DMSO.

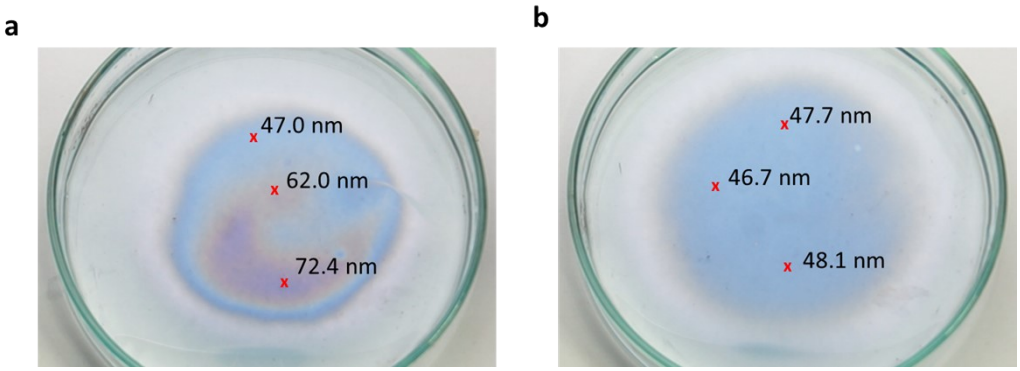

Figure S17. Spreading of the PM6 solution with CN 4% under a white LED **a)** without the DMSO, and **b)** with the DMSO 0.5%.

Light-intensity (*I*) dependence of short-circuit current and open-circuit voltage

Rough degrees of bimolecular recombination and trap-assisted recombination can be obtained via the I vs J_{SC} and I vs V_{OC}. The relationship between I and J_{SC} is described as $J_{SC} \propto I^{S}$, where S is a calculated power law exponent and explains the extent of bimolecular recombination. Figure S18a shows PB devices had lower bimolecular recombination. The relationship between I and V_{OC} is described as $V_{OC} \propto \ln I$ with a slope of nkT/q, where q is the elementary charge, T is the absolute temperature, and k is the Boltzmann constant. In this relationship, kT/q (n=1) indicates a condition where bimolecular recombination is dominant. On the other hand, 2 kT/q (a condition where trap-assisted recombination is dominant. Figure S18b shows trap-assisted recombination is lower in the PB devices.

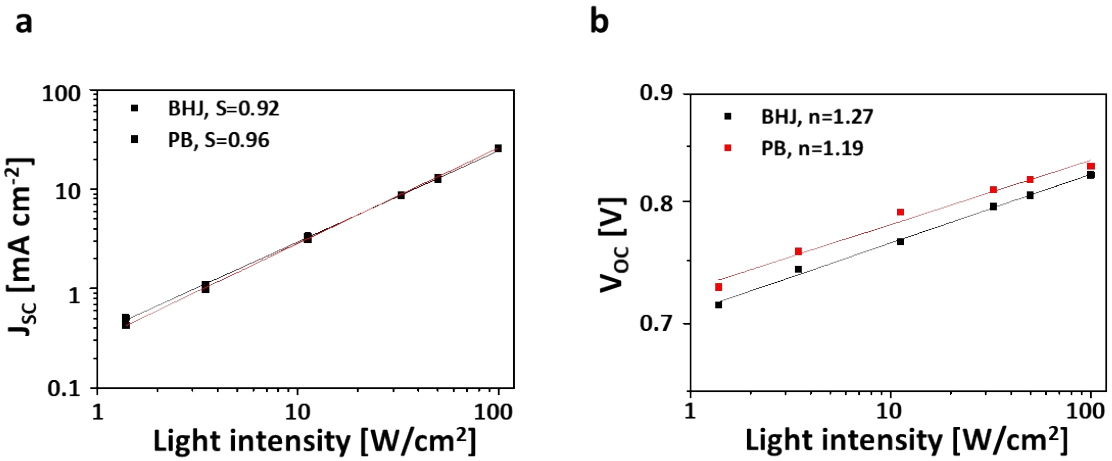

Figure S18. Responses to light intensity (I) of the BHJ and PB. **a)** J_{SC} vs. I, **b)** V_{OC} vs. I.

SCLC method for the mobility balance in the PB and BHJ OSCs

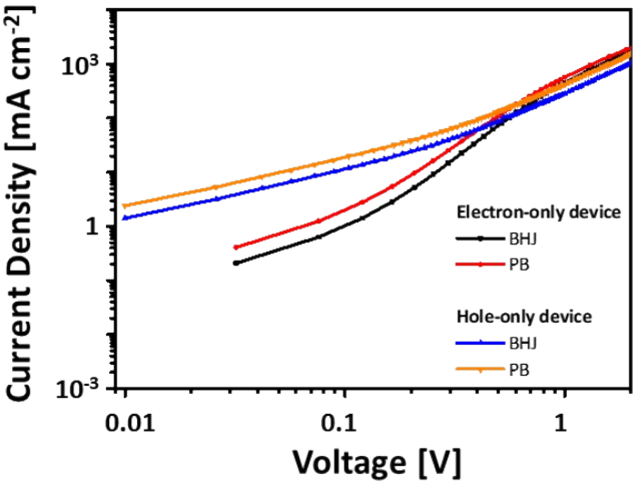

Figure S19. Dark J-V curves of hole-only devices (ITO/MoO_x/Active layer/MoO_x/Ag) and electron-only devices (ITO/ZnO/Active layer/PNDIT-F3N-Br/Ag) of the BHJ and PB for calculating mobility ratios using the SCLC method.

PL quenching and EQE

Exciton dissociation at the D/A interfaces can be seen in the photoluminescence (PL) quenching. For the PL measurement, a 514 nm light source was used and glass substrates were passivated by PNDI-F3N-Br to prevent dewetting of the films by the residual solvent (Figure S20a). The neat PM6 and Y7-BO films were coated by the SC with the same thickness (120 nm). The PL intensity of PM6 was too small to analyze the PL quenching, so we utilized the PL of Y7-BO for comparison between the BHJ and PB structure. The external

quantum efficiency (EQE) of the BHJ and PB devices was also obtained (Figure S20b). The J_{SC} values calculated by integrating the EQE in the BHJ and PB were 25.64 and 26.10 mA/cm^2, respectively.

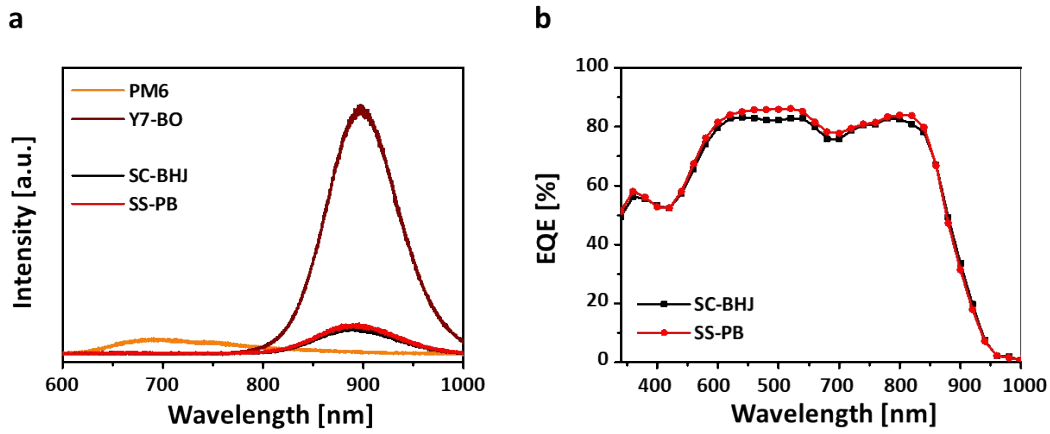

Figure S20. a) Photoluminescence (PL) and **b)** external quantum efficiency (EQE) of the BHJ and PB devices

Energy loss analysis by the FTPS-EQE measurement

Experimental V_{OC} is always different from theoretical V_{OC}, which can be expressed by energy loss ($\Delta E_{Total} = \Delta E_1 + \Delta E_2 + \Delta E_3$) (Figure S21 and Table S7). First, Shockley–Queisser (SQ) limit makes ΔE_1 by radiative recombination above bandgap, leading to ideal maximum voltage ($^{qV_{OC}^{SQ}} = E_g - \Delta E_1$). The ΔE_1 of BHJ, PB, and bilayer devices was almost the same; $^{qV_{OC}^{SQ}}$ of the bilayer devices was lower because of lower E_g by strong crystallinity compared to the BHJ and PB counterparts. Next, ΔE_2 by radiative recombination below bandgap reduces the voltage ($^{qV_{OC}^{rad}} = E_g - \Delta E_1 - \Delta E_2$). The voltage ($^{qV_{OC}^{rad}}$) of BHJ, PB, and bilayer devices became similar, because of the lower ΔE_2 of the bilayer devices by the redshift in the PL from wholly preserved crystallinity, also represented by redshift in absorption (Figure S22). Finally, non-radiative recombination reduces the voltage further ($^{qV_{OC}} = E_g - \Delta E_1 - \Delta E_2 - \Delta E_3$). The ΔE_3 was also obtained by electroluminescence (EL) measurement ($\Delta E_3 = - k_B T / q \ln(EQE_{EL})$).

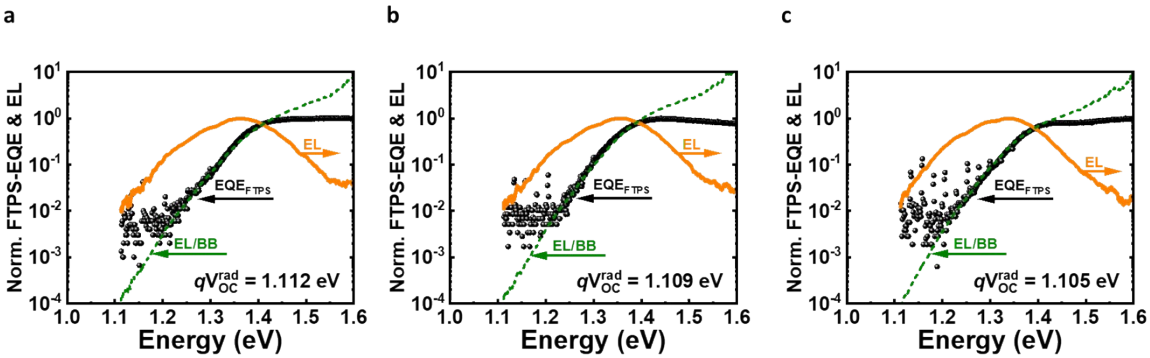

Figure S21. FTPS-EQE and EL of **a)** BHJ, **b)** PB, and **c)** bilayer devices.

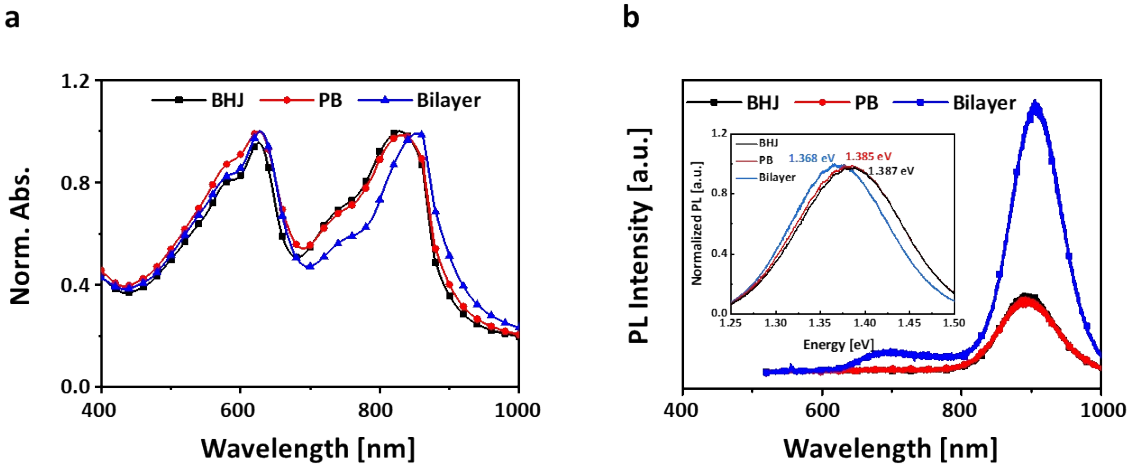

Figure S22. **a)** Absorption and **b)** photoluminescence of the BHJ, PB, and bilayer films. An inset image shows the PL peaks of the acceptors.

Air stability for operation

The PB and BHJ devices were kept in the air at room temperature for 480h (RH > 40%). The PCEs were measured at every 48h interval and normalized (Figure S23).

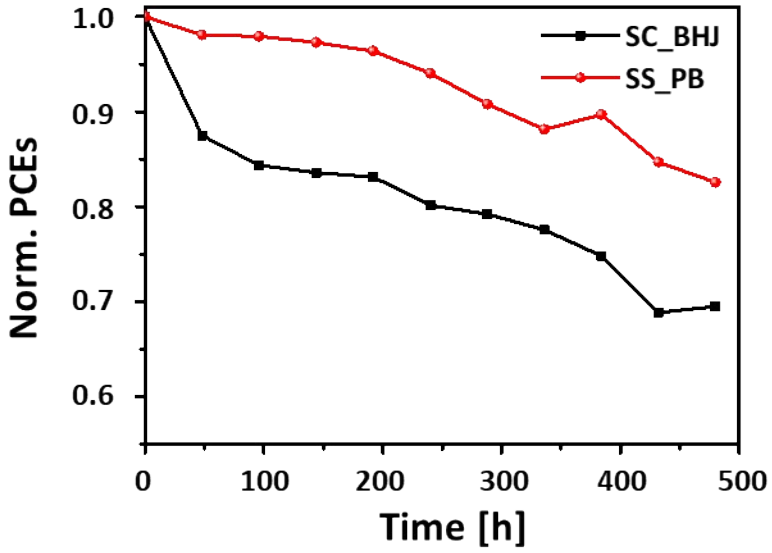

Figure S23. Degradation in normalized PCEs of BHJ and PB devices during 480h storage in ambient condition

Table S1. Parameters from the GIWAXS of the SS-PM6 films with DPE, CN and DIO

		D-spacing [Å]	CL [Å]	Face-on / edge-on
SS-PM6	No additive	3.74	20.1	0.174
	DPE 1%	3.70	34.90	0.789
	CN 1%	3.69	32.17	0.942
	DIO 1%	3.68	40	2.333

Table S2. Hole mobility from the SCLC method using hole only devices

	Mobility [cm $V^{-1}s^{-1}$]
Pristine	2.03×10^{-4}
SS_CN 0%	2.48×10^{-4}
SS_CN 1%	4.93×10^{-4}
SS_CN 4%	5.61×10^{-4}
SS_CN 7%	--

Table S3. Parameters from the GIWAXS of the SC-PM6 films with and without the CN

		D-spacing [Å]	CL [Å]	Face-on / edge-on
SC_PM6	CN 0.5%	3.7	30.68	0.47
	CN 1%	3.69	32.17	0.57
	CN 4%	3.69	35.21	0.75
	CN 7%	3.71	35.23	0.82

Table S4. Optimization of the BHJ devices by adjusting the D/A ratio and spin speed.

D:A ratio	1:1.1	1:1.3	1:1.5	1:1.7
PCE	14.43	14.51	14.58	13.41
J_{SC}	26.65	26.5	26.47	24.49
V_{OC}	0.83	0.83	0.83	0.84
FF	0.65	0.66	0.66	0.65
Spin rpm	1200 rpm	1600 rpm	2000 rpm	3000 rpm
PCE	14.58	15.01	14.93	14.2
J_{SC}	26.47	26.4	26.19	25.1
V_{OC}	0.83	0.83	0.83	0.83
FF	0.66	0.68	0.69	0.68

Table S5. Optimization of the PB devices by adjusting the annealing temperature, amount of CN, the amount of dropping solution of the PM6, and the concentration of the Y7-BO.

Annealing temperature	50℃	80℃	100℃	120℃	140℃	160℃
PCE	8.89	14.29	14.43	14.49	14.47	11.85
J_{SC}	17.26	25.25	25.04	25.07	25.01	24.38
V_{OC}	0.88	0.84	0.84	0.84	0.84	0.83
FF	0.58	0.68	0.69	0.69	0.69	0.59
Amount of CN in PM6 solution	4.40%		4.10%	3.80%		3.50%

PCE	14.23	14.48	14.72	13.78
J_{SC}	25.33	25.45	25.67	24.26
V_{OC}	0.84	0.84	0.84	0.85
FF	0.67	0.68	0.68	0.67
Dropping amount of PM6 solution	14ul	16ul	18ul	20ul
PCE	13.71	14.72	14.27	14.06
J_{SC}	24.24	25.67	25.27	24.9
V_{OC}	0.85	0.84	0.85	0.85
FF	0.67	0.68	0.67	0.66
Concentration of Y7-BO	7 mg	8.5mg	10 mg	11.5 mg
PCE	14.69	15.64	14.72	12.31
J_{SC}	25.59	25.98	25.67	24.32
V_{OC}	0.84	0.85	0.84	0.85
FF	0.68	0.71	0.68	0.60

Table S6. *J-V* parameters of OSCs for **a)** the SS-PB devices by adjusting the amount of CN in the PM6 solution, and **b)** SS-bilayer devices by adjusting the amount of CN in the PM6 solution and evaporation times of CN on the water.

a)	CN 0%	CN 1%	CN 4%	CN 7%
PCE	1.62	10.97	15.43	12.98
J_{SC}	2.96	20.97	25.52	22.31
V_{OC}	0.85	0.85	0.84	0.85
FF	0.65	0.61	0.72	0.69
b)	Bilayer w/o CN		Bilayer w/ CN, long dry	
PCE	1.62		4.44	
J_{SC}	2.96		7.42	
V_{OC}	0.85		0.89	
FF	0.65		0.67	

Table S7. Parameters form the FTPS-EQE

	E_g	qV_{OC}^{SQ}	ΔE_1	qV_{OC}^{rad}	ΔE_2	qV_{OC}	ΔE_3	$-k_BT/q \ln(EQE_{EL})$	EQE_{EL}(%)
BHJ	1.410	1.152	0.258	1.112	0.040	0.827	0.285	0.311	6.880×10^{-4}
PB	1.413	1.155	0.258	1.109	0.046	0.856	0.254	0.290	1.404×10^{-3}
Bilayer	1.383	1.127	0.256	1.105	0.022	0.871	0.234	0.254	5.425×10^{-3}

References

[1] A.D. Dussaud and S. M. Troian, *Phys. Fluids* **1998**, 10, 23

[2] J. Noh, S. Jeong, J.-Y. Lee, *Nat. Commun.* **2016**, 7, 12374

[3] V. Gencer, C. Schutz, and W. Thielemans, *Langmuir* **2017**, 33, 228

[4] Y. Tian, X. Gao, W. Hong, M. Du, P. Pan, J. Z. Sun, Z. L. Wu, and Q. Zheng, *ACS Appl. Mater. Interfaces* **2017**, 9, 34349

[5] L. Keiser, H. Bense, P. Colinet, J. Bico, and E. Reyssat, *Phys. Rev. Lett.* **2017,** 118, 074504